Synthesis and Studies on Cell-Penetrating Peptides

Jean-Remi Bertrand,[†] Claude Malvy,[†] Tiphanie Auguste,[†] Gábor K. Tóth,[‡] Orsolya Kiss-Ivánkovits,[‡] Eszter Illyés,[§] Miklós Hollósi,[§] Sándor Bottka,[||] and Ilona Laczkó*[,||]

Institute Gustave Roussy, CNRS UMR 8121, University Paris 11, Villejuif, France, Institute of Medical Chemistry, University of Szeged, Szeged, Hungary, Department of Organic Chemistry, Institute of Chemistry, Eötvös Lóránd University, Budapest, Hungary, and Institute of Plant Biology, Institute of Biophysics, Biological Research Center, Szeged, Hungary. Received January 7, 2009; Revised Manuscript Received May 13, 2009

The ability of different synthetic cell penetrating peptides, as Antennapedia (wild and Phe^6 mutated penetratins), flock house virus, and integrin peptides to form complexes with a 25mer antisense oligonucleotide was compared and their conformation was determined by circular dichroism spectroscopy. The efficiency for oligonucleotide delivery into cells was measured using peptides labeled with a coumarin derivative showing blue fluorescence and the fluorescein-labeled antisense oligonucleotide showing green fluorescence. Fluorescence due to the excitation energy transfer confirmed the interaction of the antisense oligonucleotide and cell-penetrating peptides. The most efficient oligonucleotide delivery was found for penetratins. Comparison of the two types of penetratins shows that the wild-type penetratin proved to be more efficient than mutated penetratin. The paper also emphasizes that the attachment of a fluorescent label may have an effect on the conformation and flexibility of cell-penetrating peptides that must be taken into consideration when evaluating biological experiments.

INTRODUCTION

Genomic rearrangements leading to intragenic gene fusion are found in particular types of hematopoietic malignancies and sarcomas. These chimeric genes frequently encode aberrant transcription factors, which are responsible for cellular transformation and in consequence for oncogenesis. The Ewing sarcoma (EWS) family of tumors (ESFT) belongs to this type of translocation-induced cancers (*1*). The EWS-Fli1 protein is an aberrant transcription factor that has been shown by different authors to regulate various genes. In a recent study, it was shown that, when EWS-Fli1 is specifically inhibited by a short interfering RNA (siRNA) in Ewing A673 cells, 80 genes were found up- and down-regulated, respectively, at least 2-fold (*2*). Because chromosome rearrangement occurs in the cancerous cell, the nucleic acid sequence of the junction is present only in the mRNA of tumor cells. It is, therefore, an extremely attractive target for selective therapy of Ewing sarcoma. To our knowledge, no attempts have been made to target the fusion gene at the DNA level, but antisense strategies allow for inhibition of EWS-Fli1 at the mRNA level after splicing. For this purpose, two strategies are useful: siRNA and antisense oligonucleotides (AS-ODNs).

The short interfering RNAs (siRNAs) are double-stranded oligoribonucleotides with a full duplex of 19 bases, and a 2−3-base overhang at the 3′ termini (*3, 4*). They induce the sequence-specific cleavage of mRNA in the cytoplasm by directing the RNA-induced silencing cleavage complex (RISC) to the complementary sequence on the target RNA. It is a very powerful strategy to inhibit gene expression at the RNA level, and it represents many fields of application for fundamental research. The use of siRNAs as therapeutics is in development, but some recent results show dramatic toxicity on animal models. This will require a modification of their administration ways (*5, 6*).

Antisense oligonucleotides are short, synthetic strands of DNA (or analogues) that are complementary, or antisense, to a target sequence (DNA or RNA) designed to halt a biological event, such as transcription, translation, or splicing. The mechanism of action of antisense oligonucleotides is enzymatic cleavage of the RNA strand by RNase H (*7*).

Cellular penetration is one of the main challenges to be solved for both strategies to improve their efficiency. Cationic lipids are generally used for cell application, but because of their liver capture and potential toxicity, they are limited to *in vitro* studies. Cell-penetrating virus derivative peptides have been described as molecules able to facilitate the nonendocytic membrane passage of compounds associated to them (*8*−*10*). Nevertheless, depending on the protein origin some cell penetrating peptides (CPPs) use the endocytotic pathways (*8*). The complex formation of antisense oligonucleotides with CPPs may be accomplished either by covalent coupling or by electrostatic interaction.

This paper reports the synthesis and circular dichroism (CD) studies on cell-penetrating peptides as well as epifluorescence microscopic investigation of peptide-mediated delivery of the 5′-fluorescein labeled 25mer EWS-Fli1 antisense oligonucleotide into cells. Antennapedia peptides (wild-type and Trp^6 → Phe^6 mutant penetratins) (*11, 12*), integrin sequences (*13*), and flock-house virus peptides (*14*) (Table 1) were chosen to probe the cell-penetrating efficiency of CPPs. The peptides were prepared with free N-terminus and in N-terminal fluorescent-labeled form. The 4-(7-hydroxycoumaryl)-acetyl (Hca) group served as fluorescent label (*15*). The direct interactions of the different CPPs with living cells have also been studied. Finally, their ability to deliver the fluorescein labeled AS-ODN into the cells was also measured.

MATERIALS AND METHODS

Materials. Diisopropylcarbodiimide (DIC), 1,8-diazabicyclo[5.4.0]undec-7-ene (DBU), *N,N*′-diisopropylethylamine

* Corresponding author. Ilona Laczkó, H-6726 Szeged, Temesvári krt. 62. Phone: +36-62-599608; Fax: +36-62-433133; E-mail: laczko@brc.hu.

[†] CNRS UMR 8121.

[‡] University of Szeged.

[§] Eötvös Lóránd University.

[||] Biological Research Center.

10.1021/bc900005j CCC: $40.75
Published on Web 06/25/2009

Table 1. Amino Acid Sequence, ESI-MS, and RP-HPLC Characterization of the Synthesized Peptides[a]

peptides	numbering	MW calcd	MW [MH^+] found	RP-HPLC R_t
	Penetratins			
H-RQIKI**W**FQNRRMKWKK-NH_2	**1**	2244.3	2245.7	24.2[b]
Hca-RQIKI**W**FQNRRMKWKK-NH_2	**1a**	2446.3	2447.2	19.5
H-RQIKI**F**FQNRRMKWKK-NH_2	**2**	2206.3	2206.8	23.1[b]
Hca-RQIKI**F**FQNRRMKWKK-NH_2	**2a**	2408.3	2408.6	18.5[c]
	Integrin Peptides			
H-SRYDDSVPRYHAVRIRKEEREIKDEK-NH_2	**3**	3272.7	3273.6	14.9[d]
Hca-SRYDDSVPRYHAVRIRKEEREIKDEK-NH_2	**3a**	3476.6	3477.0	18.9[d]
H-LEAEKERRKSGLSS-NH_2	**4**	1587.9	1588.8	18.3[b]
Hca-LEAEKERRKSGLSS-NH_2	**4a**	1789.1	1789.9	22.4[c]
	FHV Peptides			
H-ASMWERVKSIIKSSLAAASNI-NH_2	**5**	2261.2	2261.8	26.0[c]
Hca-ASMWERVKSIIKSSLAAASNI-NH_2	**5a**	2462.2	2463.6	27.5[c]
H-IGVAASGISGLSALFEGFGF-NH_2	**6**	1898.3	1899.3	28.8[c]
Hca-IGVAASGISGLSALFEGFGF-NH2	**6a**	2101.0	2101.4	32.0[c]

[a] Eluent A: 0.08% TFA/H_2O; B: 0.064% TFA/MeCN-H_2O (95:5, v/v), flow rate: 1 mL/min. [b] Gradient 5−50% B in 25 min. [c] Gradient 15−70% B in 30 min. [d] Gradient 5−60% B in 25 min.

(DIEA), hydrogen fluoride (HF), 1-hydroxybenztriazole (HOBt), and trifluoroacetic acid (TFA) were obtained from Fluka. Trifluoroethanol (TFE, Uvasol, Merck, for spectroscopy) was used for CD neasurements. Acetonitrile (MeCN), dichloromethane (DCM), and dimethylformamide (DMF) are from Reanal (Budapest, Hungary). Boc-amino acid derivatives and 4-methyl benzhydrylamine resin were from Bachem (Bubendorf, Switzerland). 4-(7-Hydroxycoumaryl)acetic acid (Hca) was prepared by the method of Baker et al. (*15*). Dulbecco's modified Eagle's medium (DMEM), newborn calf serum, and penicillin−streptomycin solution were purchased from Gibco. Trizol was purchased from Invitrogen and RNasin from Promega.

Oligonucleotide. The 5′-fluorescein labeled 25mer EWS-Fli1 AS-ODN is targeted toward the junction sequence between EWS and Fli1 genes as described by Tanaka et al. (*16*) and corresponds to the nucleotides 832−856. EWS-Fli1 AS-ODN inhibits proliferation of human Ewing's sarcoma and primitive neuroectodermal tumor cells (*16*−*18*). To protect it from nuclease degradation, all phosphate groups were changed into phosphorothioate. The AS-ODN sequence 5′-GACTGAGT-CATAAGAAGGGTTCTGC-3′ was provided by Eurogentec (Belgium), HPLC-purified and mass spectrometry controlled. A control phosphorothioate sequence (Ct-ODN) was used for the PCR studies with the following sequence: 5′-GCAGAAC-CCTTCTTATGACTCAGTC-3′

The EWS-Fli1 AS-ODN, without fluorescein label, was synthesized with an Expedite 8909 synthesizer (Applied Biosystems, USA), using solid-supported standard β-cyanoethyl phosphoramidite chemistry at a nominal scale of 1 μmol. Purification was performed by HPLC on a Kromasil 100-C18 250 × 10 mm ID column, using a MeCN 0.1 M triethylammonium acetate (pH 7.0) mixture as eluent. This results in the triethylammonium salt of ODN.

Peptide Synthesis. Peptides (Table 1) were synthesized by manual solid-phase methodology, using Boc/Bzl strategy (*19*) and 4-methyl benzhydrylamine resin (0.7 mmol/g). All amino acids were coupled as Boc-derivatives. The amino acid side chain protection was the following: Boc-Asn(Xan)-OH, Boc-Asp(OcHex)-OH, Boc-Arg(Tos)-OH, Boc-Gln(Xan)-OH, Boc-Glu(OcHex)-OH, Boc-His(Tos)-OH, Boc-Lys-(2ClZ)-OH, Boc-Ser(Bzl)-OH, Boc-Trp(For)-OH [xan (xanthyl), cHex (cyclohexyl), Tos (tosyl), 2ClZ (2-Cl-benzyloxycarbonyl), Bzl (benzyl), For (formyl)]. The Hca coupling was performed by using the DIC/HOBt method (3 equiv of each) (*20*). The coupling efficacy was monitored by the ninhydrin (*21*) assay. Boc-groups were removed by 35% TFA in DCM. Neutralization together with the removal of the formyl-group of Trp was carried out with DBU/piperidine before the final cleavage from the resin with HF containing *p*-cresol as scavenger at 0 °C for 1.5 h. The crude products were analyzed and purified by reverse-phase HPLC as described below.

High-Performance Liquid Chromatography. Analytical RP-HPLC (Jasco, Japan) was performed using an Alltech Alltima C18 WP column (250 × 5 mm) with 5 μm particle size and 300 Å pore size. Depending on peptide composition (Table 1), a linear gradient elution was developed from 5−50% eluent B in 25 min, 15−70% eluent B in 30 min, or 5−60% B in 35 min; eluent A is 0.08% TFA in water and eluent B is 0.064% TFA in acetonitrile−water (95−5%). Detection was performed at 220 and 280 nm. Experiments were carried out at a flow rate of 1 mL/min, at ambient temperature. Samples were applied at 0.1 mg/0.1 mL concentration in eluent A. Purification of peptides was achieved on an Alltech Alltima C18 WP column (250 × 25 mm) with 5 μm particle size and 300 Å pore size using gradient elution with the same eluents, 10 mL/min flow rate, and 20 mg/mL sample concentration. Homogeneity of the pure peptides was confirmed by analytical RP-HPLC.

Electrospray Ionization Mass Spectrometry (ESI-MS). The identification of the peptides was achieved by mass spectrometry (*20*). Electrospray ionization mass spectrometry was performed with a Bruker Daltonics Esquire 3000 Plus (Bremen, Germany) mass spectrometer, operating in continuous sample injection at 4 μL/min flow rate. Samples were dissolved in 50% acetonitrile−water mixture. Mass spectra were recorded in positive mode in the *m*/*z* 200−1500 range. R_f values of purified peptides, calculated, and found masses are listed in Table 1.

Circular Dichroism Spectroscopic Studies. CD spectra were recorded on a Jasco J-810 dichrograph (calibrated with ammonium *d*-10-camphor sulfonate) at room temperature using a 0.02 cm cell for measurements when TFE/water was used as solvent. All measurements are the average of four scans, and the resolution was 0.2 nm. The concentration of the peptides ranged from 0.5 to 1 mM depending on the absorption. The conformational change of penetratins **1** and **2** and the FHV peptide **5** was also monitored in the presence of 5 mM aqueous anionic micelles [L-α-lysophosphatidylcholine (LPC) to L-α-lysophosphatidylserine (LPS) molar ratio (r_M) was 9]. The concentration of the peptides was in this case 40 μM, and a 0.1 cm cell was used.

The CD spectra of AS-ODN and peptide-(AS-ODN) complexes were recorded in the range 250−320 nm in a 0.1 cm cell. The AS-ODN concentration in the samples was in each case 20 μM, and the peptide concentration varied in the interval

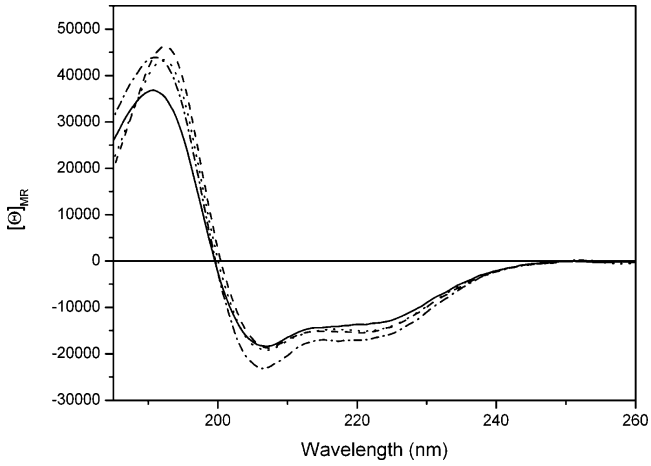

Figure 1. Far-UV CD spectrum of penetratins **1** (—), **1a** (-•-•-), **2** (---), and **2a** (•••) in TFE:water, 9:1 (v/v).

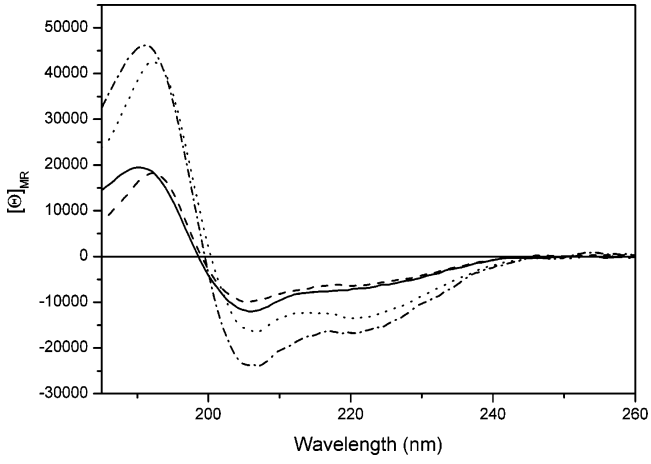

Figure 2. Far-UV CD spectrum of penetratins **1** (—), **1a** (-•-•-), **2** (---), and **2a** (•••) TFE/water, 1:1 (v/v).

20−200 μM. Prior to scanning, the AS-ODN was incubated with the peptides for 1 h. The CD spectra were expressed as mean residue ellipticity $[\Theta]_{MR}$ and were given in units of deg cm^2 dmol^{-1}, using a mean residue weight of 114 for the peptides and 306 for the ODN.

Including the free N-terminus, the wild-type (**1**) and mutant penetratin (**2**) comprise eight basic groups but no acidic ones. The Hca-labeled peptides **1a** and **2a** comprise one less basic side-chain group. With this taken into account, the penetratin peptides **1** and **2** bind eight, **1a** and **2a** seven, trifluoroacetic acid molecules that significantly increase their molecular mass. Quantitative amino acid analysis of the penetratin peptides resulted in peptide contents which agreed with the decreased values calculated from the molecular mass of peptide−TFA salts. In the case of peptides **3**−**6**, the TFA content was calculated for the net positive charge (number of basic residues minus number of acidic residues). The $[\Theta]_{MR}$ values were calculated for the increased molecular mass.

AS-ODN Delivery to Cells. NIH/3T3 cells stably transformed by EWS-Flil oncogene (NIH/3T3-EF) were grown in DMEM medium supplemented by 10% heat-inactivated newborn calf serum and penicillin−streptomycin solution. The cells were seeded into 6-well plate at 2 × 10^5 cell in 1 mL of medium and grown at 37 °C with 5% CO_2 in a moist atmosphere before treatment. Twenty-four hours later, the medium was discarded and replaced by 900 μL of new one. Fluorescein-labeled AS-ODN (0.5 nmol) was incubated for 10 min in 100 μL of 100 mM NaCl, 10 mM Hepes buffer, pH 7.2 containing 17 nmol of

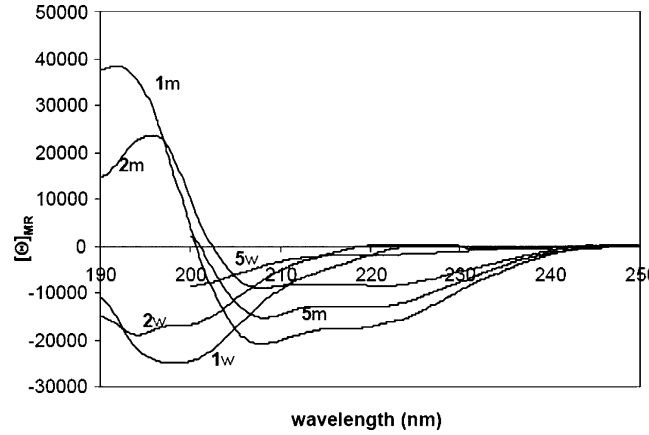

Figure 3. Far-UV CD spectrum of peptides **1**, **2**, and **5** in water (curves 1w, 2w, 5w) and in the presence of 5 mM aqueous anionic micelles (LPC/LPS, r_M = 9) (curves 1m, 2m, 5m). Peptide concentration was 40 μM.

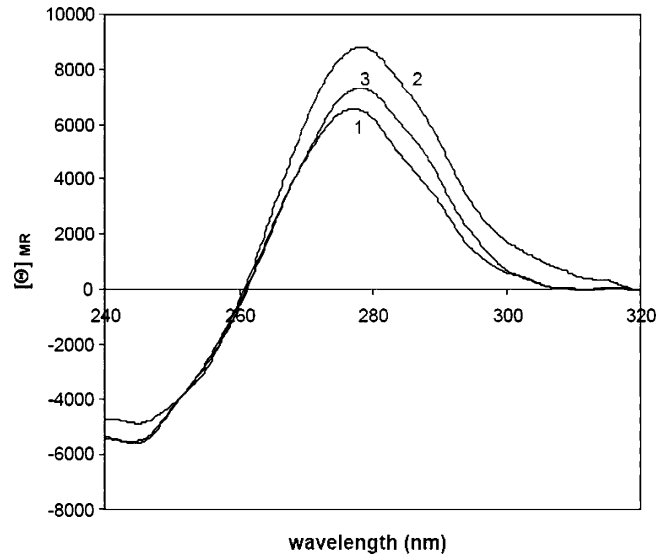

Figure 4. Near-UV CD spectrum of AS-ODN (curve 1), associates of (AS-ODN)-wild-type penetratin (curve 2), and (AS-ODN) mutant penetratin (curve 3) in water. Peptide/ODN, r_M = 2.5.

peptide **1a** or **2a**, 15 nmol of peptide **3a**, 30 nmol of peptide **4a**, and 40 nmol of peptide **5a** or **6a** (arbitrary value because these latter peptides do not contain any cationic amino acid) to obtain a charge ratio (r_{CH}) of 5 (positive charges of peptide vs the negative charges of ODN). The charge ratio of 5 has been selected from previous studies (*22, 23*). The complexes were then added to the cells and incubated for 3 h. The cells were washed two times with a PBS solution, treated with a 4% formaldehyde solution in PBS for 20 min, washed two times with PBS, and observed under epifluorescence microscopy (*24*) (Axiovert 100, Zeiss) with a CCD camera. The same cell treatments were performed with the Hca-peptides alone at 50 μM or the fluorescent AS-ODN alone at 500 nM final concentrations. Fluorescence was observed using an emission multiwavelength filter (460/10, 530/25, 625/50 nm, maximum/band-pass). For the detection of the Hca blue light and the fluorescein green light emission, excitation filters of 365/12 and 494/17 were used, respectively.

Determination of EWS-Fli1 Expression by RT-PCR. The NIH/3T3-EF cells were grown in 6 well plates and seeded one day before the treatment with (AS-ODN)−peptide complexes at 3 × 10^5 cells/mL in DMEM containing 10% newborn calf serum, 100 U/mL streptomycin, and 100 μg/mL penicillin. After

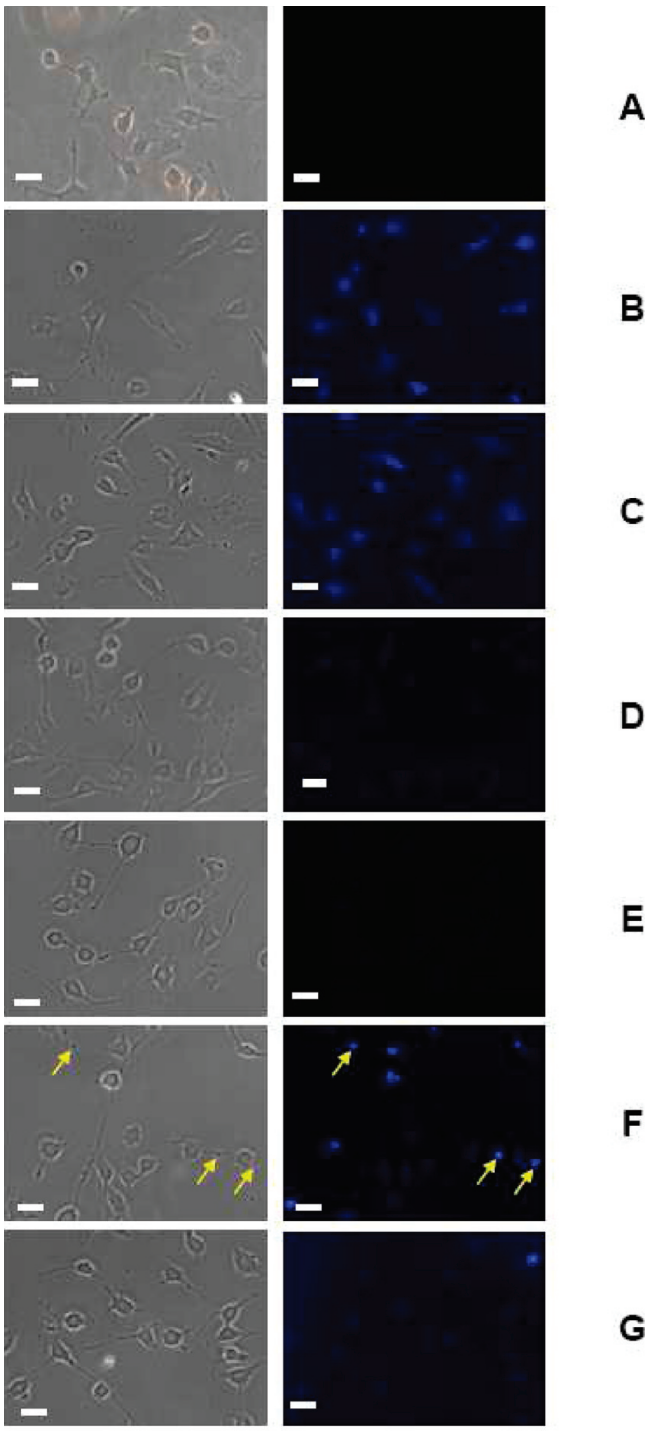

Figure 5. Interaction of peptides with cells. NIH/3T3 cells, incubated for 3 h alone (A) or with 50 μM wild-type penetratin **1a** (B); mutated penetratin **2a** (C); integrin peptide **3a** (D); integrin peptide **4a** (E); FHV peptide **5a** (F); and FHV peptide **6a** (G). The cells were observed with white light (left panel) or excitating Hca at 365 nm (right panel) to detect the different Hca-labeled peptides. Scale bar is 20 μm.

24 h treatment, the cells were washed with PBS buffer (Gibco) and then lysed with 800 μL Trizol, 130 μL of chloroform/isoamylalcohol (49:1, v/v). After centrifugation at 13 000 rpm for 15 min, 350 μL of the aqueous phase was precipitated with an aquivalent volume of isopropanol. Total RNA were then collected by centrifugation at 13 000 rpm for 15 min, washed two times with 75% ethanol solution, and air-dried. The RNA pellet was solved in 10 μL water containing 0.5 U/μL of RNasin, and the solution concentration was determined by absorption spectroscopy. The cDNA was produced on 1 μg of total RNA after hybridization with 2 μL of random primer 50 μg/mL (Promega) in 14.5 μL final volume by heating the solution for 5 min at 65 °C. The cDNA synthesis is performed for 1 h at 42 °C after addition of 4 μL of 5× more concentrated buffer (Biolabs), 0.5 μL 20 mM dNTP, 0.5 μL RNasin 40 U/μL, and 0.5 μL Mo-MuLV reverse transcriptase (Biolabs) 200 U/μL. PCR reaction was performed on 2 μL of cDNA prepared as described above, 5 μL of 10-fold concentrated buffer (Biolabs), 0.5 μL 20 mM dNTP, 0.5 μL of each primer 50 μg/mL, and 0.5 μL of Taq DNA polymerase 5 U/μL (Biolabs). Primer sequences are EWS-Fli1 forward 5′-AGC-AGT-TAC-TCT-CAG-CAG-AAC-AAC-3′ and reverse 5′-CCA-GGA-TCT-GAT-ACG-GAT-CTG-GCT-G-3′. G3PDH was used as the housekeeping gene, and the sequence of the corresponding primers is forward 5′-CAT-TGT-CAT-ACC-AGG-AAA-TC-3′. Amplification conditions were as follows: (i) fusion 94 °C (30 s), (ii) hybridization 56 or 63 °C (30 s) for EWS-Fli1 or G3PDH, respectively, and (iii) elongation 72 °C (50 s). The amplified fragments were detected on 2% agarose gel electrophoresis in TAE buffer and ethidium bromide staining with a CCD camera and corresponding gel analysis system (Ingenius, Syngene).

RESULTS AND DISCUSSION

Circular Dichroism Spectroscopy. The conformational preferences and the effect of fluorescent labeling upon conformation of peptides were probed by CD spectroscopy. The spectra were taken in TFE/water 9:1 (v/v), TFE/water 1:1 (v/v) mixtures, and water. (The wild-type penetratin peptide **1** is not soluble in neat TFE.) TFE is a helix promoting solvent; it is frequently used to mimic cell membranes or their vicinity (*25*). Figure 1 shows the effect of N-terminally coupled Hca-group on the conformation of wild-type (**1**) and mutant (**2**) penetratin in TFE/water, 9:1. The spectrum of **1** is characteristic of peptides featuring high helix content. The phenylalanine-containing mutant peptide **2** also shows a typical helix-type CD spectrum in the same solvent mixture, but the intensity of the positive band at 192.5 nm is higher than that of **1** at 190.5 nm, while the negative bands are less intense. The flock-house virus (FHV) sequence **5** shows a CD spectrum reflecting lower helicity (spectra not shown). As reference, the CD spectra of two integrin sequences **3** and **4** were also measured in TFE. The band amplitudes in the spectrum of the longer sequence **3** are larger as a sign of higher helicity of the 26-mer peptide (spectra not shown).

It is an intriguing question whether or not the attachment of the fluorescent label 4-(7-hydroxycoumaryl)-acetyl (Hca) group has an effect upon the conformation of the peptide. In the far-UV spectrum of 4-(7-hydroxycoumaryl)-acetic acid (Hca-OH), two bands appear at 198 nm ($A = 3.28 \times 10^4$) and 217.5 nm ($A = 1.24 \times 10^4$). Thus, the Hca-group is expected to have a CD spectral effect in the far-UV region if the conformational movement of the N-terminus of the peptide is restricted. As shown in Figure 1, the Hca-group increases the intensity of both the negative and positive bands of wild-type penetratin (**1a**), but it does not have a significant effect upon the spectrum of the mutant penetratin (**2a**). The Hca-group has an effect only on the negative bands in the CD spectrum of the FHV peptide [λ_{nm} ($[\Theta]_{MR}$) values in TFE/water (9:1) for **5**, 218 (−13 240), 207 (−15 200), 190 (26 500), and **5a**, 221 (−11 200), 207 (−12 700), 190.5 (26 200)].

On the basis of the higher band intensities of the exciton couplet in the region of $\pi-\pi^*$ transition, the mutant penetratin **2** shows a more expressed tendency to adopt a helical structure than the wild-type peptide **1**. The attachment of the Hca-group stabilizes the helical conformation of **1** likely through $\pi-\pi$ interaction between the indole ring of tryptophan and the hydroxycoumaryl group at the N-terminus. They are located in

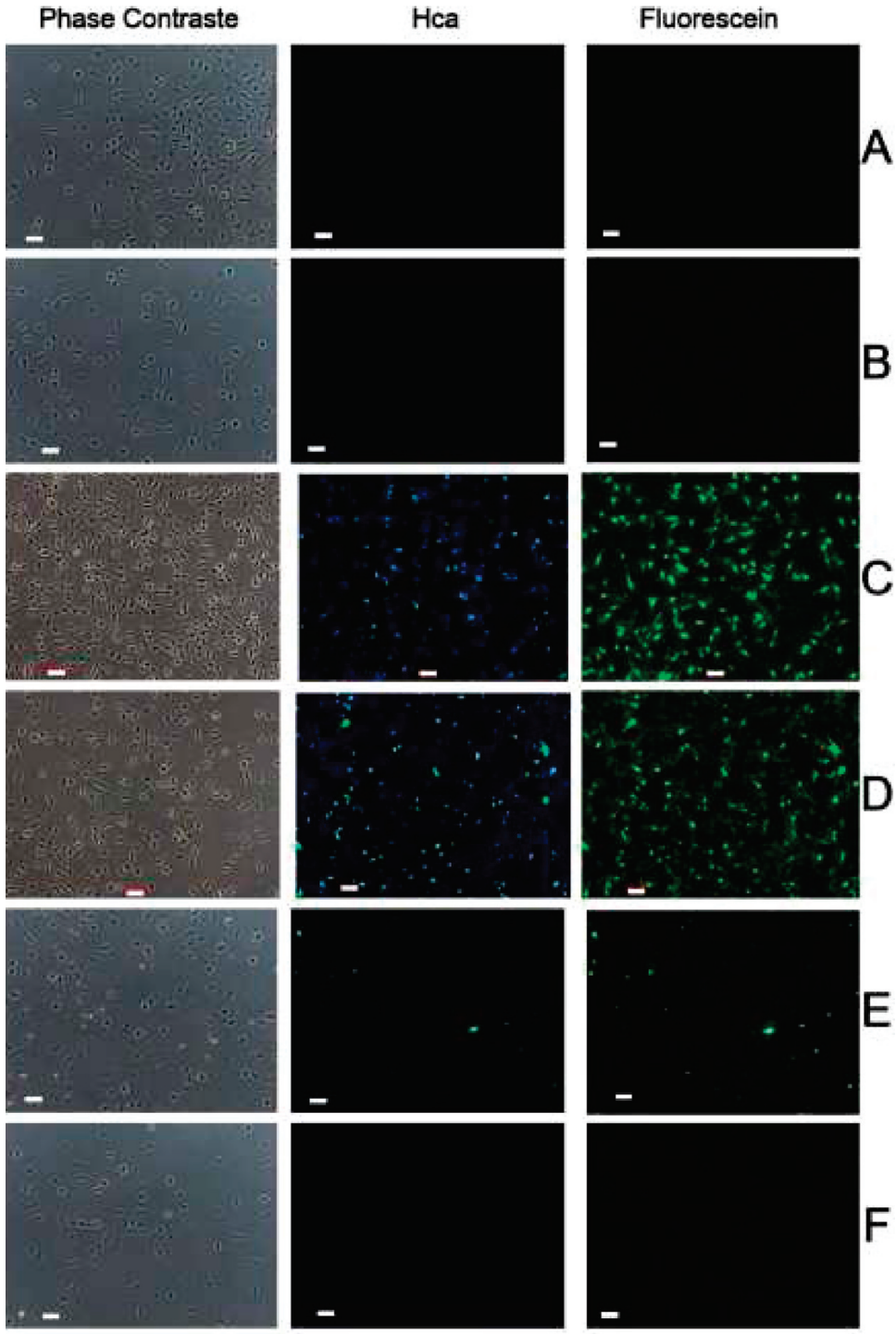

Figure 6. Oligonucleotide interactions with NIH/3T3 cells transformed by EWS-Flil ncogene. Cells incubated for 3 h alone (A); or with 500 nM fluorescein labeled AS-ODN (B); the same labeled AS-ODN complexes to wild-type penetratin **1a** (C); mutated penetratin **2a** (D); FHV peptide **5a** (E); and FHV peptide **6a** (F). The cells were observed with white light (left panel) or exciting Hca at 365 nm (middle panel) and fluorescein at 494 nm (right panel) to detect the interaction between cells and AS-ODN. Fluorescence emission was observed using a three band-pass filter on color camera as described in Materials and Methods. Scale bar is 20 μm.

sterically close position on the same side of the helix cylinder. The phenyl group of phenylalanine in **2** cannot effectively interact with the coumarin ring.

The relative stability of the helices of **1**, **1a**, **2**, and **2a** was probed by measuring their CD spectra in TFE/water 1:1 (v/v). The helical structure of the Hca-penetratins **1a** and **2a** is more resistant to the effect of aqueous environment than that of **1** or **2** (Figure 2). In water, **1**, **2**, and **5** show CD spectra reflecting dominantly unordered conformation (Figure 3). More interestingly, CD spectra in Figure 3 demonstrate that peptides **1**, **2**, and **5** are prompted to adopt α-helical conformation in aqueous solution in the presence of anionic micelles (LPC/LPS, r_M = 9). The induced helicity is more expressed for the wild-type **1** than for the mutant penetratin **2** (Figure 3).

On the basis of CD studies reported earlier, the wild-type penetratin **1** and the FHV peptide **5** interact with an 18-mer AS-ODN in water and in the presence of anionic micelles (*26*). The 25-mer AS-ODN used in this study was found to form complexes with both **1** and **2** (Figure 4). However, the spectral change in the near UV region, characteristic of ODN, is more

pronounced in the presence of **1** than **2** at peptide to ODN molar ratio $r_M = 2.5$. (Above these ratios, the solutions become opaque as a sign of aggregate formation that obscures the measurements of CD.)

Interaction of Hca-Peptides with Cells. NIH/3T3 EWS-Fli1 cells treated by the Hca-peptides were observed under epifluorescence microscopy taking advantage of the blue emission of Hca under UV excitation (365 nm). No fluorescence was observed for untreated cells (Figure 5A) Both the wild-type (**1a**) and mutated (**2a**) penetratin peptides were found to interact strongly with the cells (Figure 5B,C) with a cytoplasmic and nuclear localization. The mutant peptide **2** was earlier described as an inefficient cell-penetrating peptide (*24*). The association of these positively charged peptides to the cells is probably due to electrostatic interaction with the negatively charged cell membrane. Although confocal microscopy could not be used for the detection of Hca fluorescence because of the lack of laser with an emission band corresponding to Hca, the blue fluorescence observed at the nucleus position indicated that the peptides did enter the cell. If the peptides were localized on the cytoplasmic membrane, a pericellular flourescence would have been observed.

The fusogenic region of FHV (**5a**) interacts weakly with the cells with a cytoplasmic localization (Figure 5F). The intense fluorescence spots observed in this case correspond to peptide aggregates located on the external side of membranes as indicated by the yellow arrows on the left panel (bright field) and right panel (fluorescence) slides. The RNA binding peptide sequence (**6a**) of FHV has a low solubility and forms aggregates, which interact unspecifically with dead cells (Figure 5G). The Hca−integrin peptides (**3a** and **4a**) do not interact efficiently with the cells in our experimental conditions (Figure 5D,E).

Peptide-Mediated Delivery of AS-ODN into Cells. To determine the ability of the peptides to facilitate the AS-ODN penetration, cells were incubated for 3 h with fluorescein-labeled AS-ODN (500 nM) alone or in the presence of different peptides ($r_{CH} = 5$; see Materials and Methods). After incubation of AS-ODN with peptides **1a**, **2a**, or **5a**, we observed that the solutions became opalescent, probably due to formation of complexes between the AS-ODN and peptides. No green fluorescence was observed under epifluorescence microscopy of untreated NIH/3T3 cells expressing EWS-Flil oncogene (Figure 6A). After cell treatment with 500 nM AS-ODN for 3 h, a fraction of cells displayed a weak fluorescence (Figure 6B).

The Antennapedia derivative peptides can both make the AS-ODN penetrate into the cells (Figure 6C,D) independently of the mutation. The AS-ODN has mainly a cytoplasmic localization. The higher intensity of the fluorescein emission in Figure 6C compared to Figure 6D indicated that **1a** peptide is much more efficient for AS-ODN delivery than **2a**. This is consistent with an earlier finding where the wild-type penetratin was 2× more efficient for ODN delivery than the Phe^6 mutant penetratin (*25*). The blue fluorescence corresponding to the peptide **1a** and **2a** was still detected on cells after the complex was formed between peptide and AS-ODN. Nevertheless, the fluorescence intensity was much higher compared to that when the cells were treated only with the peptides (compare Figure 5B to Figure 6C and Figure 5C to Figure 6D) suggesting a cooperation between peptides and ODN for interaction with cells.

It can be seen in Figure 6C,D that all the cells present green and blue fluorescence indicating that peptides **1a** and **2a** are very efficient in interaction with the cells and in AS-ODN transfer. Observation of the cells with higher magnification (Figure 7) confirms these results.

Surprisingly, when the slides were illuminated using a filter of 365 nm for exciting Hca we observed green dots in the medium and in the cell membrane level (Figures 6C,D and Figure 7). (This is possible because the emission filter possesses three band passes: blue, green, and red). It is known that if the fluorescence emission spectrum of a donor molecule and the absorption spectrum of an acceptor molecule overlap excitation energy transfer occurs. The intensity of this transfer is inversely proportional to the square of distance between the donor and the acceptor molecules. The wavelength maximum of the emission spectrum of Hca is 460 nm (*20*), and that of the excitation spectrum of fluorescein is 494 nm; hence upon formation of complex between the AS-ODN and the peptide, an increased emission of the fluorescein at 530 nm was observed illuminating the slides at the excitation wavelength (365 nm) of Hca (Figure 6C,D and Figure 7). These complexes are mainly localized on the bottom of the plate (Figure 7, yellow arrow) or on the cell membrane (Figure 7, white arrow). The amount of complex localized on the membrane is higher for peptide **1a** than for **2a**. This means that membrane localization for peptide **1a** is not only of statistical origin. Figure 7 shows that no fluorescence transfer occurs in the cell-bound complex [under Hca fluorescence condition (excitation at 365 nm), the cells are blue]. This result indicates that after interaction with the cell membrane the complexes are dissociated, that is, AS-ODNs and the peptides are located at a large distance that excludes fluorescence transfer. The dissociation is probably favorable for the antisense activity of AS-ODNs.

Integrin peptides **3** and **4** are not able to cause efficient penetration of the AS-ODN into cells (results not shown). The

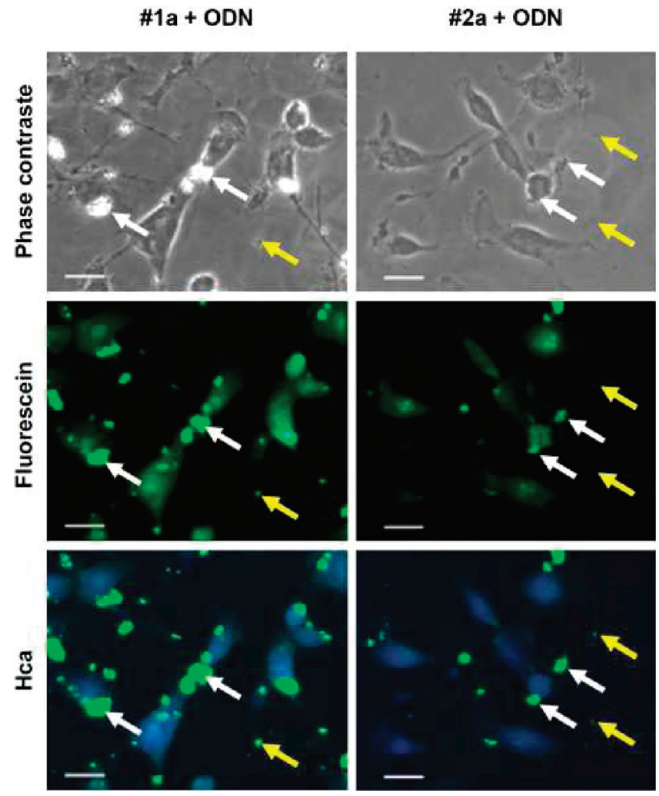

Figure 7. Oligonucleotide interactions with NIH/3T3 cells transformed by EWS-Fli1 oncogene. The cells were incubated for 3 h with 500 nM fluorescein labeled (AS-ODN)-wild-type penetratin **1a** or (AS-ODN)-mutated penetratin **2a** complexes. The cells were observed with white light (top panel) or exciting the fluorescein at 494 nm (middle panel) and Hca at 365 nm (bottom panel) to detect the interaction between cells and AS-ODN. Fluorescence emission was observed using a three band-pass filter on color camera as described in Materials and Methods. Arrows indicate the position of the (AS-ODN)-peptide aggregates: white arrows show aggregates localized on the bottom of the plate; yellow arrows show aggregates localized on cell membrane. Scale bar is 20 μM.

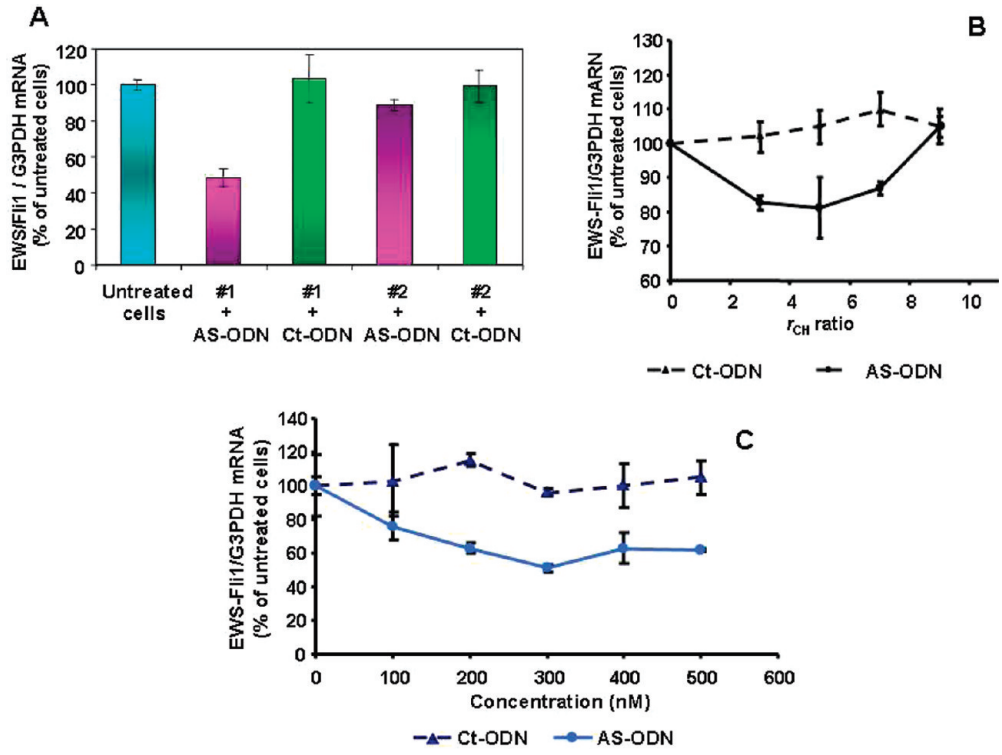

Figure 8. Inhibition of EWS-Fli1 mRNA expression in NIH/3T3-EF cells by antisense ODN (As-ODN) or control sequence (Ct-ODN). (A) The ODN is vectorized by wild-type (**1**) or mutated (**2**) penetratins. Measurement was performed by RT-PCR. ODN concentration was 500 nM and $r_{CH} = 5$. (B) Influence of the r_{CH} ratio on AS-ODN penetration into cell by wild-type penetratin **1**. The cells were treated for 24 h with 200 nM ODN and peptide **1** with r_{CH} varying from 0 to 9. (C) Dose effect of ODN vectorized by wild-type peptide **1** at $r_{CH} = 5$ on EWS-Fli1 expression in cell after 24 h treatment. Gene expression is determined by RT-PCR.

AS-ODN fluorescence intensity is the same that observed for AS-ODN alone and may be attributed to a nonspecific ODN interaction with cell membranes.

The FHV derived peptide **5a** corresponding to the fusogenic part of the protein causes a weak penetration of the AS-ODN into cells (Figure 6E). Fluorescence transfer is observed in aggregates close to the cells (similarly to that found with **1a** and **2a**) indicating the formation of complexes between AS-ODN and peptide **5a** (Figure 6E). The peptide **6**, bearing no positive charges, does not form a complex with the AS-ODN (Figure 6F).

According to CD studies (Figure 1), the attachment of the Hca-group increases the helicity of the wild-type penetratin, while the Hca-group weakly decreases the helicity of the mutant peptide. Anionic micelles induce helicity in the case of both **1** and **2** peptides, which is a more expressed for **1** than **2** (Figure 3). On the basis of CD studies, the wild-type penetratin **1** has a more flexible conformation than the mutant **2**, which is likely more favorable for ODN binding and cell penetration.

Inhibition of EWS-Fli1 Expression by AS-ODN Vectorized by Antennapedia Derivative Peptides. The ability of wild-type and mutated Antennapedia peptides to vectorize efficiently AS-ODN into cells was studied by the measurement of targeted oncogene expression. After cell treatment, total RNA is extracted, and EWS-Fli1 mRNA expression is measured by RT-PCR. It can be seen in Figure 8 that wild-type penetratin is able to inhibit EWS-Fli1 expression only if associated to the AS-ODN. In the same condition, control ODN has no effect. These results indicate that the lower transfection efficiency of mutated penetratin is correlated with the loss of gene inhibition. It has been proposed that association of penetratin peptides to the cell membrane is due to electrostatic interactions. The conformational change of penetratin upon $Trp^6 \rightarrow Phe^6$ mutation must be responsible for the decrease of cell penetration. Indeed, it has been described that the $Gln^8 \rightarrow Pro^8$ change presents a similar effect confirming the key role of this domain for the cell penetration (*27*).

The efficiency of transfection of nucleic acids by noncovalently linked CPP is largely dependent on the ratio of charges (r_{CH}) between the two components. The inhibition of EWS-Fli1 expression determined by PCR was performed for different ODN to CPP charge ratio ($r_{CH} = 0-9$) using the wild-type Antennapedia peptide **1**. Figure 8B shows that maximum inhibition was obtained for r_{CH} ratio of 5 confirming the results obtained previously (*22, 23*). Dose-dependent treatment (Figure 8C) of the cells shows a maximum inhibition at 300 nM in As-ODN associated to peptide **1**. Under the same conditions, the Ct-ODN displays no inhibition, confirming the specificity of the treatment. For higher concentrations, the efficiency of inhibition was not increased, probably because aggregate formation between the ODN and the peptide might take place. This is unfavorable for ODN delivery and may be associated with a toxic effect.

SUMMARY

Antennapedia peptides were previously described as efficient agents for the delivery of oligonucleotides either by covalent linking or through ionic interaction (*28, 29*). The action has been attributed to a conformational change of the molecule when interacting with the membrane. The introduction of a mutation inside this peptide was found to result in a dramatic decrease in oligonucleotide delivery. Surprisingly, in our hands both the wild-type and mutated peptides interact strongly with cells (Figure 5). The CD spectra of the wild (**1**) and mutated (**2**) penetratins in TFE solution show that the helicity of the mutated peptide is higher than that of the wild-type, while the Hca-labeled penetratins show similar CD spectra (as a sign of comparable helix content) and interaction with cells (Figure 6). It is likely that the increased helicity of the membrane-bound

wild-type Hca-penetratin (**1a**) explains its improved ability to cross the cell membrane. It should be emphasized here that the attachment of a fluorescent label may have an effect on the conformation and the flexibility of cell-penetrating peptides that must be taken into consideration when evaluating biological experiments.

ACKNOWLEDGMENT

This work was supported by the following grants: CNRS exchange convention with Hungary; European STREP Prothets devoted to Ewing Sarcoma to J.-R.B. and C.M.; NI 68466 to M.H.; RET108/2004 to I.L.

LITERATURE CITED

(1) Maksimenko, A., and Malvy, C. (2005) Oncogene-targeted antisense oligonucleotides for the treatment of Ewing sarcoma. *Expert Opin. Ther. Targets 9*, 825–830.

(2) Prieur, F., Tirode, P., Cohen, O., and Dellatre, O. (2004) EWS/Fli-1 silencing and gene profiling of Ewing cells reveal downstream oncogenic pathways and a crucial role for repression of insulin-like growth factor binding protein 3. *Mol. Cell. Biol. 24*, 7275–7283.

(3) Elbashir, S. M., Harborth, J., Lendeckel, W., Yalcin, A., Weber, K., and Tuschl, T. (2001) Duplexes of 21-nucleotide RNAs mediate RNA interference in cultured mammalian cells. *Nature 411*, 494–498.

(4) Elbashir, S. M., Lendeckel, W., and Tuschl, T. (2001) RNA interference is mediated by 21-and 22-nucleotide RNAs. *Genes Dev. 15*, 188–200.

(5) Couzin, J. (2006) Molecular biology - RNAi safety comes under scrutiny. *Science 312*, 1121–1124.

(6) Frantz, S. (2006) Safety concerns raised over RNA interference. *Nat. Rev. Drug Discovery 5*, 528–529.

(7) Crooke, S. T. (2004) Progress in antisense technology. *Annu. Rev. Med. 55*, 61–95.

(8) Fischer, P. M. (2007) Cellular uptake mechanisms and potential therapeutic utility of peptidic cell delivery vectors: Progress 2001−2006. *Med. Res. Rev. 27*, 755–795.

(9) Pujals, S., Fernandez-Carneado, J., Lopez-Iglesias, C., Kogan, M. J., and Giralt, E. (2006) Mechanistic aspects of CPP-mediated intracellular drug delivery: Relevance of CPP self-assembly. *Biochim. Biophys. Acta 1758*, 264–279.

(10) Patel, L. N., Zaro, J. L., and Shen, W. C. (2004) Cell penetrating peptides: intracellular pathways and pharmaceutical perspectives. *Pharm. Res. 24*, 1977–1992.

(11) Derossi, D., Joliot, A., Chassaing, G., and Prochiantz, A. (1994) The third helix of the Antennapedia homeodomain translocates through biological membranes. *J. Biol. Chem. 269*, 10444–10450.

(12) Lindgren, M., Hällbrink, M., Prochiantz, A., and Langel, Ü. (2000) Cell-penetrating peptides. *Trends Pharmacol. Sci. 21*, 99–103.

(13) Tamura, R. N., Rozzo, C., Starr, L., Chambers, J., Reichardt, L. F., Cooper, H. M., and Quaranta, V. (1990) Epithelial integrin alpha-6beta-4 - complete primary structure of alpha-6 and variant forms of beta-4. *J. Cell Biol. 111*, 1593–1604.

(14) Bong, D. T., Janshoff, A., Steinem, C., and Ghadiri, R. M. (2000) Membrane partitioning of the cleavage peptide in flock house virus. *Biophys. J. 78*, 839–845.

(15) Baker, W., Haksar, C. N., and McOmie, J. F. N. (1950) Fluorescent reagents. Acyl chlorides and acyl hydrazides. *J. Chem. Soc.* 170–174.

(16) Tanaka, K., Iwakuma, T., Harimaya, K., Sato, H., and Iwamoto, Y. (1997) EWS-Fli1 antisense oligodeoxynucleotide inhibits proliferation of Human Ewing's sarcoma and primitive neuroectodermal tumor cells. *J. Clin. Invest. 99*, 239–247.

(17) Lambert, G., Bertrand, J.-R., Fattal, E., Subra, E. F., Pinto-Alphandary, H., Malvy, C., Auclair, C., and Couvreur, P. (2000) EWS Fli-1 antisense nanocapsules inhibits Ewing sarcoma-related tumor in mice. *Biochem. Biophys. Res. Commun. 279*, 401–406.

(18) Toub, N., Bertrand, J.-R., Malvy, C., Fattal, E., and Couvreur, P. (2006) Antisense oligonucleotide nanocapsules efficiently inhibit EWS-Fli1 expression in a Ewing's sarcoma model. *Oligonucleotides 16*, 158–168.

(19) Stewart, J. M., and Young, J. D. (1984) *Solid Phase Peptide Synthesis*, Pierce Chemical Company, Rockford, IL.

(20) Kele, P., Illyés, E., Mezõ, G., Dóda, M., Mák, M., Kaposi, D. A., and Sebestyén, F. (1999) Fluorescent derivatives of bovine neurotensin 8−13 fragment. *Lett. Pept. Sci. 6*, 225–238.

(21) Kaiser, E., Colescott, R. L., Bossinger, C. D., and Cook, P. I. (1970) Color test for detection of free terminal amino groups in solid-phase synthesis of peptides. *Anal. Biochem. 34*, 595–598.

(22) Toth, J., Böszörményi, I., Majer, Zs., Laczkó, I., Malvy, C., Hollósi, M., and Bertrand, J.-R. (2002) A two step model aimed at delivering antisense oligonucleotides in targeted cells. *Biochem. Biophys. Res. Commun. 293*, 18–22.

(23) Laczkó, I., Váró, Gy., Bottka, S., Bálint, Z., Illyés, E., Vass, E., Bertrand, J.-R., Malvy, C., and Hollósi, M. (2006) N-terminal acylation of the SV40 nuclear localization signal peptide enhances its oligonucleotide binding and membrane translocation efficiencies. *Arch. Biochem. Biophys. 454*, 146–154.

(24) Dom, G., Shaw-Jackson, C., Matis, C., Bouffioux, O., Picard, J. J., Prochiantz, A., Mingeot-Leclercq, M. P., Brasseur, R., and Rezsohazy, R. (2003) Cellular uptake of Antennapedia Penetratin peptides is a two-step process in which phase transfer precedes a tryptophan-dependent translocation. *Nucleic Acid Res. 31*, 556–561.

(25) Jackson, M. and, and Mantsch, H. H. (1992) Halogenated alcohols as solvents for proteins: FTIR spectroscopic studies. *Biochim. Biophys. Acta 1118*, 139–143.

(26) Laczkó, I., Bottka, S., Tóth, G. K., Malvy, C., Bertrand, J.-R., and Hollósi, M. (2004) Interaction of fusogenic peptides with an antisense oligonucleotide in solution and in the presence of micelles: conformational studies. *Biochem. Biophys. Res. Commun. 313*, 356–361.

(27) Lindgren, M., Gallet, X., Soomets, U., Hallbrink, M., Brakenhielm, E., Pooga, M., Brasseur, R., and Langel, U. (2000) Translocation properties of novel cell penetrating transportan and penetratin analogues. *Bioconjugate Chem. 11*, 619–626.

(28) Mäe, M., and Langel, Ü. (2006) Cell-penetrating peptides as vectors for peptide, protein and oligonucleotide delivery. *Curr. Opin. Pharmacol. 6*, 509–514.

(29) Veldhoen, S., Laufer, S. D., Trampe, A., and Restle, T. 2006: Cellular delivery of small interfering RNA by a non-covalently attached cell-penetrating peptide: quantitative analysis of uptake and biological effect. *Nucleic Acids Res. 34*, 6561–6573.

BC900005J